Supporting Information: X-ray Reflectivity Reveals a Non-monotonic Ion-Density Profile Perpendicular to the Surface of $ErCl_3$ Aqueous Solutions

Guangming Luo,[1, §] Wei Bu,[2] Miroslav Mihaylov,[2] Ivan Kuzmenko,[3] Mark L. Schlossman[2] and L. Soderholm[1,*]

[1] *Chemical Sciences and Engineering Division, Argonne National Laboratory, Argonne, Illinois 60439, USA*

[2]*Department of Physics, University of Illinois at Chicago, Chicago, Illinois 60607, USA*

[3]*Advanced Photon Source, Argonne National Laboratory, Argonne, Illinois 60439, USA*

[§]Current Address: *BSRF, Institute of High Energy Physics, Chinese Academy of Sciences, Beijing, 100049, China*

$ErCl_3$ Manufacturer's Certificate of Analysis

Alfa Aesar, Erbium (III) chloride hydrate, Reaction, 99.99% (REO), Stock Number 11305, Lot Number, L11R002: Values in ppm, Na 2; Mg <1; Al 5; Si 4; K <1; Ca 3; Sc <1; Ti <1;V <1; Cr <1;Mn <1; Fe 1; Ni <1; Cu <1; Zn <1;Y <1; La <1; Ce <1; Pr <1; Nd <1; Sm <1; Eu <1; Gd 10; Tb <1; Dy <1; Ho 2; Tm <1; Yb <1; Lu <1;Hg <1; Pb <1; Bi <1; Th <0.4; U <0.2.

X-ray Results and Analysis

A model-independent Patterson function analysis of the data is presented that does not assume an *a priori* functional form for the electron density profile. The results of the Patterson function analysis reveal the essential features of the electron density profile that are included in the model which is used in the main paper to fit the X-ray reflectivity data. Also presented is an additional analysis of the model for the intrinsic surface-structure factor that is discussed in the main paper.

Patterson function analysis. Calculation of the interfacial Patterson function is a model-independent method to extract interfacial structural information from X-ray reflectivity. The interfacial Patterson function $P(s)$ is the autocorrelation function of the gradient $\rho_\infty^{-1}\,\partial\rho(z)/\partial z$ and is calculated directly from the measured data $R(Q_z)/R_F(Q_z)$,[1-2]

Eq. S 1 $$P(s) \equiv \frac{1}{\rho_\infty^2}\int dz\ \frac{\partial\rho(z)}{\partial z}\ \frac{\partial\rho(s+z)}{\partial z} = \frac{1}{2\pi}\int dQ_z\ \frac{R(Q_z)}{R_F(Q_z)}\,e^{-iQ_z s}$$

Calculation of the Fourier transform requires an assumption for values of $R(Q_z)/R_F(Q_z)$ over the range of Q_z that is larger than the maximum measured value $Q_{z,max} = 0.86$ Å^{-1}. The only assumption is that capillary wave fluctuations of the surface must effect the X-ray reflectivity

measurements at all values of Q_z. To do this, the values of $R(Q_z)/R_F(Q_z)$ for $Q_z > Q_{z,max}$ are extended with a Gaussian falloff whose width is the capillary roughness of the surface (calculated for the maximum wave vector transfer $Q_{z,max}$). This assumption will affect the shape of the Patterson function only for values of s on the order of $1/Q_{z,max} \approx 1.2$ Å, where s is the distance from the surface in the z-direction. Note that a hard cutoff at $Q_{z,max} = 0.86$ Å^{-1} would introduce oscillations with a wavelength of $2\pi/0.86 \approx 7$ Å, which, as shown below, do not appear in our $P(s)$.

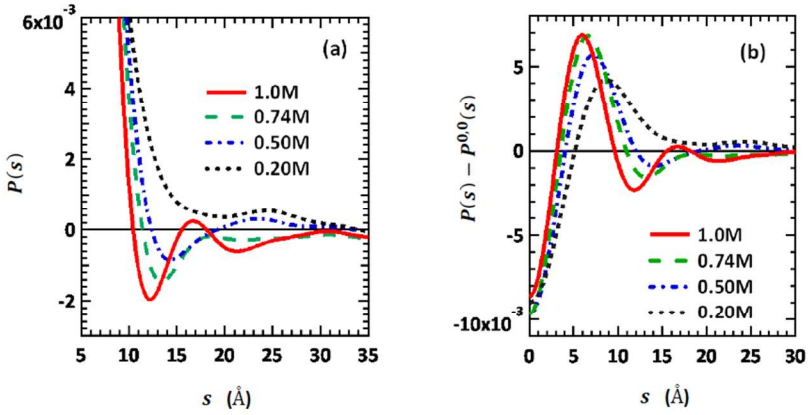

Figure S1 (a) Patterson function, $P(s)$, for the water/vapor interfaces of 0.20 M, 0.50 M, 0.74 M and 1.0 M $ErCl_3$ solutions. (b) $P(s) - P^{0,0}(s)$ for the same samples as in (a), where $P^{0,0}(s)$ models the solution/vapor interface without any interfacial structure as a simple step-function interface with interfacial roughness that is calculated from the measured surface tension.

Figure S1a shows the interfacial Patterson function $P(s)$ obtained for samples of 0.20 M, 0.50 M, 0.74 M, and 1.0 M $ErCl_3$ concentration. The oscillations that appear in $P(s)$ represent interfacial structure, which varies with concentration. These oscillations can be interpreted using Eq. S1 to demonstrate the existence of a peak in electron density between 5 Å and 9 Å from the surface, depending upon the concentration, and an additional peak between about 15 Å and 20 Å for the two highest concentrations. One method to reveal this interfacial structure from $P(s)$ is to express the electron density profile as $\rho(z) = \rho^0(z) + \rho^\delta(z)$, where $\rho^0(z)$ is the interfacial electron density of a simple step-function interface with capillary roughness such that $(1/\rho_\infty)(\partial\rho^0(z)/dz) = G_{cap}(z)$ (where $G_{cap}(z) = (\sqrt{2\pi}\sigma_{cap})^{-1}\exp[-z^2/(2\sigma_{cap}^2)]$), and $\rho^\delta(z)$ is the difference between the real electron density profile $\rho(z)$ and $\rho^0(z)$. Eq. S1 is rewritten in terms of the auto-correlation functions of ρ^0, ρ^δ and their cross-correlations $P^{0,0}(s)$, $P^{\delta,\delta}(s)$ and $P^{0,\delta}(s)$,

Eq. S2 $$P(s) = P^{0,0}(s) + 2P^{0,\delta}(s) + P^{\delta,\delta}(s)$$

$$P^{0,0}(s) = \frac{1}{\rho_\infty^2}\int dz \cdot \frac{\partial \rho^0(z)}{\partial z} \cdot \frac{\partial \rho^0(s+z)}{\partial z} = \frac{1}{2\sqrt{\pi}\sigma_{cap}} \exp[-s^2/(4\sigma_{cap}^2)]$$

$$P^{0,\delta}(s) = \frac{1}{\rho_\infty^2}\int dz \cdot \frac{\partial \rho^0(z)}{\partial z} \cdot \frac{\partial \rho^\delta(s+z)}{\partial z}$$

$$P^{\delta,\delta}(s) = \frac{1}{\rho_\infty^2}\int dz \cdot \frac{\partial \rho^\delta(z)}{\partial z} \cdot \frac{\partial \rho^\delta(s+z)}{\partial z}$$

Figure S1b illustrates $P(s) - P^{0,0}(s)$, *i.e.*, the Patterson function $P(s)$ obtained from the reflectivity data minus $P^{0,0}(s)$, where $P^{0,0}(s)$ is a calculated function that models the solution/vapor interface as a simple error-function interface (without ion or molecular ordering) that includes interfacial roughness. The quantity $P(s) - P^{0,0}(s)$ is, therefore, results from the ion and molecule ordering near the interface.

Since the average electron density of the solution is much greater than the variation resulting from ion ordering, the autocorrelation function $P^{\delta,\delta}$ is small and $P(s) - P^{0,0}(s) \approx P^{0,\delta}(s)$, which is the cross-correlation between $\frac{1}{\rho_\infty}\frac{\partial \rho^0}{\partial z}$ and $\frac{1}{\rho_\infty}\frac{\partial \rho^\delta}{\partial z}$ (Eq. S2). Recalling that $\frac{1}{\rho_\infty}\frac{\partial \rho^0}{\partial z}$ is a positive Gaussian function with an $\sim$5 Å full width centered at $z = 0$, the positive-going zero-crossings in $P(s) - P^{0,0}(s)$ represent minima in the electron density profile that have a spatial extent of at least 5 Å . Therefore Figure S1b indicates that ρ^δ is negative close to the surface. This aspect corresponds to the depletion layer discussed in the main paper. Similarly, negative-going zero crossings in $P(s) - P^{0,0}(s)$ represent maxima in the electron density profile. The position of the first negative-going zero crossing for each concentration indicates that a maximum in electron density occurs at progressively larger values of z as the concentration is reduced. The higher concentration samples have multiple positive- and negative-sloped zero-crossings that represent alternating minima and maxima in the electron density profile. Note that the positions of the zero-crossings correspond only approximately to the positions of maxima or minima in the electron density profiles. This model-independent analysis of the data is consistent with the real space model of the electron density profile that is presented in the main paper.

Further Analysis of the Reflectivity Data Using the Surface Structure Factor from the Main Paper

Figure S2a shows a further analysis of the 1.0 M data in order to illustrate which pieces of the model described in Eq. 2 are responsible for the minimum in the reflectivity. The factor $|\Phi(Q_z)|^2$ can be written as

Eq. S3
$$|\Phi(Q_z)|^2 \equiv \left|\frac{1}{\rho_\infty}\int_{-\infty}^{\infty} dz \frac{\partial \rho_{int}(z)}{\partial z} exp[iQ_z z]\right|^2$$
$$= 1 + 2Re[\Phi_d(Q_z) + \Phi_{osc}(Q_z)] + 2Re[\Phi_c(Q_z)]$$

where the second term in Eq. 2 of the main paper is written as

Eq. S4 $$\Phi_d(Q_z) = \tilde{\rho}_d\left(1 - e^{iQ_z d}\right),$$

and the third term in Eq. 2 is written as

Eq. S5 $$\Phi_{osc}(Q_z) = -iQ_z \frac{\rho_{osc}}{\rho_\infty} \frac{2\pi/\Lambda}{(2\pi/\Lambda)^2 + (\Gamma^{-1} - iQ_z)^2} e^{iQ_z d} \equiv \Phi^s_{osc}(Q_z)\, e^{iQ_z d},$$

and

Eq. S6 $$Re[\Phi_c(Q_z)] = \tfrac{1}{2}\{|\Phi_d(Q_z)|^2 + |\Phi_{osc}(Q_z)|^2 + 2Re[\Phi_d(Q_z)\, \Phi_{osc}(Q_z)]\}.$$

Figure S2a shows that the primary contribution to the minimum in the reflectivity data is due to the oscillatory part of the structure factor $\Phi_{osc}(Q_z)$ that describes the Er^{3+} ion layering. By displaying $\Phi^s_{osc}(Q_z)$ defined in Eq. (10), which does not displace the oscillations (the Er^{3+} ion layers) from the vapor interface, Figure S2b shows that the minimum would occur at a lower value of Q_z than the measured value ($Q_z = 0.65$ Å^{-1}) if the depletion layer is not present. The data requires the Er^{3+} ion layering to be displaced from the surface by a distance d. This displacement is accomplished by the phase factor $e^{iQ_z d}$ in the expression for $\Phi_{osc}(Q_z)$.

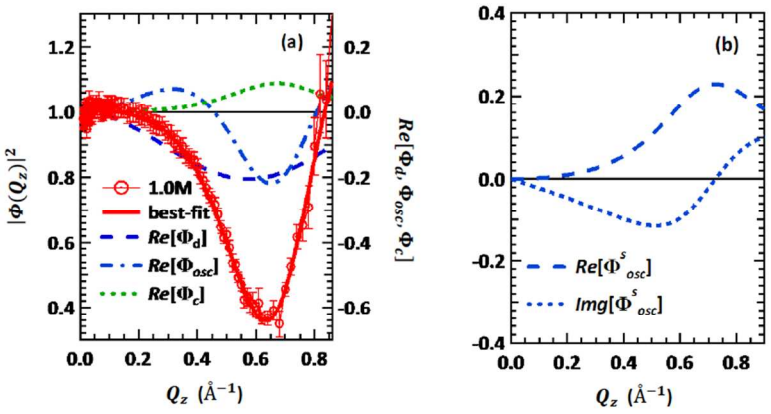

Figure S2. (a) A fit (solid line) of the model intrinsic surface structure factor $|\Phi(Q_z)|^2$ in Eq. 2 to the reflectivity data from the 1.0 M $ErCl_3$ solution/vapor interface (circles). The long dashed line illustrates $Re[\Phi_d(Q_z)]$ (Eq. S4) for the layer depleted of Er^{3+} ions, the dashed-dotted line illustrates $Re[\Phi_{osc}(Q_z)]$ (Eq. S5) for the oscillatory structure that represents the layering of Er^{3+} ions, and the dotted line shows the real part of the cross-term, $Re[\Phi_c(Q_z)]$ (Eq. S6). These real parts can be combined to construct $|\Phi(Q_z)|^2$, as demonstrated in Eq. S3. (b) Real and imaginary parts of $\Phi^s_{osc}(Q_z)$ (Eq. S5). Note that neither term has a minimum in $|\Phi(Q_z)|^2$ near $Q_z = 0.65$ Å^{-1}.

Thickness dependence of the depletion layer. The fitting of the data in the main paper is very sensitive to the thickness of the Er-depleted layer. Figure S3 demonstrates this sensitivity by displaying the best fits when the thickness of the depletion layer is fixed to the values $d =$

1 Å, 3 Å, 5 Å and 7 Å, and the other parameters (ρ_d, $\rho_{osc} > 0$, Λ, Γ) are varied. Note that ρ_{osc} has been defined to be positive such that the oscillatory part of the structure factor represents the positive adsorption of Er^{3+} ions. A peak at small Q_z that does not appear in the data is produced by the model if the depletion layer is too thin ($d = 1$ Å and 3 Å). Figure S3 also shows that values of d slightly larger than the best-fit value of 5.5 Å, such as $d = 7$ Å, yield a poor fit near the minimum at $Q_z = 0.65$ Å^{-1}.

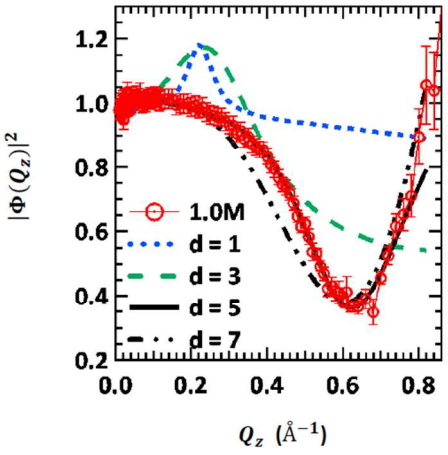

Figure S3. Fits of the model intrinsic surface structure factor $|\Phi(Q_z)|^2$ to the reflectivity data obtained from the 1.0 M $ErCl_3$ solution/vapor interface (circles) for different fixed values of the thickness d of the Er-depleted region. The fits are obtained by adjusting the other parameters (ρ_d, $\rho_{osc} > 0$, Λ, and Γ) to achieve a best fit. Thickness $d = 1$ Å (dotted line), $d = 3$ Å (dashed line), $d = 5$ Å (solid line) and d=7 Å (dashed-dotted line). The best fit to the 1.0 M data illustrated in Figure 1 has a $d = 5.5$ Å.

Molecular dynamics[3-7]

Potentials. Here, we provide additional information on the potentials used for the implicit solvent MD simulation. We use effective short-range ion interactions that are determined by Molina *et al.* from all-atom MD simulations of lanthanides in bulk aqueous solutions, specifically, the average short-range pair potentials of Ln^{3+}- Ln^{3+}, Ln^{3+}-Cl^-, and Cl^-- Cl^- shown in Figure 4 of their paper.[8] Here, Ln^{3+} refers to an average lanthanide that was calculated by Molina *et al.* as an average over their results for La^{3+}, Nd^{3+}, Eu^{3+}, Dy^{3+}, and Lu^{3+}.[8] We utilize their results by analytically approximating their pair potentials by the following function, where this short-range potential is truncated at 12 Å.

Eq. S7

$$U = \begin{cases} \varepsilon_1\left(\frac{\sigma}{r-r_0}\right)^m - \varepsilon_2\left(\frac{\sigma}{r-r_0}\right)^n + U_{osc} & r > r_0 \\ \infty & r \le r_0 \end{cases}$$

$$U_{osc} = \begin{cases} \varepsilon_3 \sin\left(\frac{r-r_1}{d} + \varphi_0\right) \exp\left[-\left[\left(r-r_1\right)/\zeta\right]^p\right] & r > r_1 \\ 0 & r \le r_1 \end{cases}$$

The parameters used in Eq. S7 are: Cl^-- Cl^- interaction potential: $m = 9$, $n = 6$, $\varepsilon_1 = 3.0\ kT$, $\varepsilon_2 = 1.5\ kT$, $r_0 = 1.5$ Å, $\sigma = 2.8$ Å, $\varepsilon_3 = -0.6\ kT$, $r_1 = 4.2$ Å, $d = 2.8$ Å, $\zeta = 2.8$ Å, $p = 3$, $\varphi_0 = 0$. Ln^{3+}-Cl^- interaction potential: $m = 6$, $n = 2.5$, $\varepsilon_1 = 1.9\ kT$, $\varepsilon_2 = -0.8\ kT$, $r_0 = 1.2$ Å, $\sigma = 3.4$ Å, $\varepsilon_3 = -1.6\ kT$, $r_1 = 4.4$ Å, $d = 2.4$ Å, $\zeta = 2.2$ Å, $p = 2$, $\varphi_0 = 0$. Ln^{3+}-Ln^{3+} interaction potential: $m = 6$, $n = 2$, $\varepsilon_1 = 1.28\ kT$, $\varepsilon_2 = -0.614\ kT$, $r_0 = 6$ Å, $\sigma = 1.2$ Å, $\varepsilon_3 = 0$. This approximation produces the pair potentials shown in Figure S4, which capture the essential features of the pair-potentials computed by Molina et al.[8]

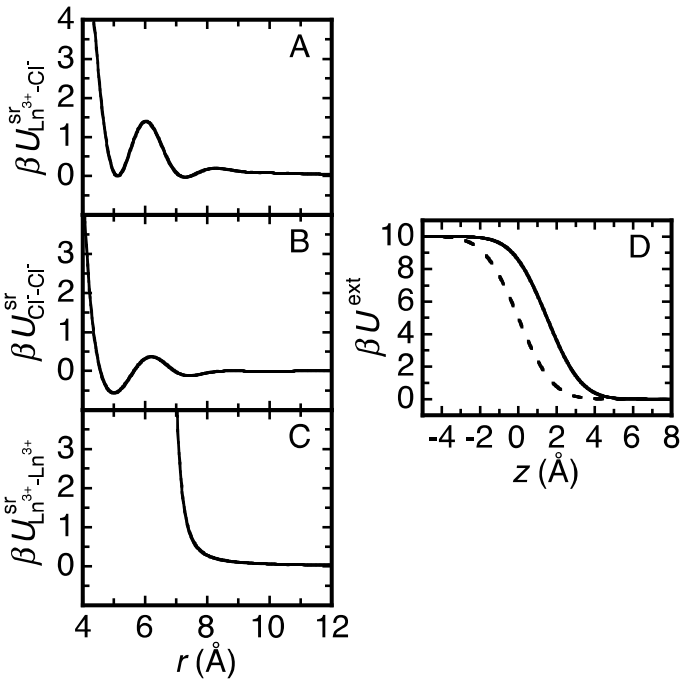

Figure S4. Coarse-grained short-range pair potentials used in MD simulation, modeled upon those in Figure 4 of Ref. [8], as described in the text. The average lanthanoid, Ln^{3+}, represents the Er^{3+} ions investigated experimentally. (a) Ln^{3+} - Cl^- (b) Cl^- – Cl^-, (c) Ln^{3+}– Ln^{3+} pair potentials, (d) surface boundary potentials for the Ln^{3+} (solid line) and Cl^- (dashed line), U^{ext}, that confine the ions inside the slab in the z-direction.

Since an implicit solvent does not have solvent molecules that can phase separate into a liquid and a vapor phase, the water surface is modeled by surface boundary potentials for the cation and anion, U^{ext}, that confine the ions inside the slab in the z-direction (see Figure S4d). The surface boundary potential of Ln^{3+} is chosen to be 1.5 Å deeper than that of Cl^-, as shown in the figure, in order to model the effect of the strong hydration shell of the trivalent Ln^{3+}, though results of the simulation are not qualitatively different when this displacement is varied.

Image Charges. The electrostatic interactions of ions with the dielectric discontinuity of a water surface are modeled by image charges calculated about the *z*=0 surface position (see Fig. 3). The electrostatic interactions, including image charge interactions, between two ions A and B near a surface can be written as

Eq. S8 $$U_{AB}^{im} = \frac{1}{\varepsilon}\left[\frac{q_A q_B}{r_{AB}} + \frac{q_A q_{A\prime}}{r_{AA\prime}} + \frac{q_B q_{B\prime}}{r_{BB\prime}} + \frac{q_A\, q_{B\prime}}{r_{AB\prime}} + \frac{q_{A\prime}\, q_B}{r_{A\prime B}}\right]$$

where $q_{A\prime}$ and $q_{B\prime}$ are the image charges of q_A and q_B, with their coordinates $r_{A\prime}$ and $r_{B\prime}$ respectively, $r_{AB} = |\mathbf{r}_A - \mathbf{r}_B|$. When the surface about which the image is taken is located at z_0, the coordinate $\mathbf{r}_A \equiv (x_A, y_A, z_A)$ is related to $\mathbf{r}_{A\prime} \equiv (x_{A\prime}, y_{A\prime}, z_{A\prime})$ by $x_{A\prime} = x_A$, $y_{A\prime} = y_A$ and $z_{A\prime} = 2z_0 - z_A$. The interaction can be considered as a sum of interactions between 4 charges, q_A, q_B, $q_{A\prime}$ and $q_{B\prime}$, excluding the interaction between $q_{A\prime}$ and $q_{B\prime}$. The force can be written as

Eq. S9 $$\mathbf{F}_{AB}^{im}(\mathbf{r}_A) \equiv -\frac{dU_{AB}^{im}}{d\mathbf{r}_A} = -\frac{\partial U_{AB}^{im}}{\partial \mathbf{r}_A} - \frac{\partial U_{AB}^{im}}{\partial \mathbf{r}_{A\prime}} \cdot \frac{d\mathbf{r}_{A\prime}}{d\mathbf{r}_A}$$

For a slab with two image surfaces (the top and bottom of the slab), the interaction between two ions can be written as

Eq. S10 $$U_{AB}^{slab,im} = \frac{1}{\varepsilon}\left[\frac{q_A q_B}{r_{AB}} + \frac{q_A q_{A\prime}}{r_{AA\prime}} + \frac{q_B q_{B\prime}}{r_{BB\prime}} + \frac{q_A\, q_{B\prime}}{r_{AB\prime}} + \frac{q_{A\prime}\, q_B}{r_{A\prime B}} + \frac{q_A q_{A\prime\prime}}{r_{AA\prime\prime}} + \frac{q_B q_{B\prime\prime}}{r_{BB\prime\prime}} + \frac{q_A\, q_{B\prime\prime}}{r_{AB\prime\prime}} + \frac{q_{A\prime\prime}\, q_B}{r_{A\prime\prime B}}\right]$$

where $\prime$ and $\prime\prime$ represent the charges imaged from the two surfaces. The force can be written as

Eq. S11 $$\mathbf{F}_{AB}^{slab,im}(\mathbf{r}_A) \equiv -\frac{dU_{AB}^{slab,im}}{d\mathbf{r}_A} = -\frac{\partial U_{AB}^{slab,im}}{\partial \mathbf{r}_A} - \frac{\partial U_{AB}^{slab,im}}{\partial \mathbf{r}_{A\prime}} \cdot \frac{d\mathbf{r}_{A\prime}}{d\mathbf{r}_A} - \frac{\partial U_{AB}^{slab,im}}{\partial \mathbf{r}_{A\prime\prime}} \cdot \frac{d\mathbf{r}_{A\prime\prime}}{d\mathbf{r}_A}$$

Without image charges, the electrostatic interaction energy of a 2d periodic slab with *N* ions is

Eq. S12 $$U^{slab} = \sum_m \sum_{i=0}^{N} \sum_{j\neq i} \frac{1}{2} \frac{q_i q_j}{|\mathbf{r}_i - \mathbf{r}_j - \mathbf{R}_m|}$$

where $\mathbf{R}_m$ is the *m*th periodic vector of the slab cell. The summation on the right side can be calculated with the SPME method.[4-7, 9-10] With image charges, the electrostatic interaction of the slab can be written as

Eq. S13 $$U^{slab,im} = U^{slab,ri1} + U^{slab,ri2} - U^{slab} - U^{slab,i1} - U^{slab,i2}$$

The five right-hand terms (labeled (1) – (5) from left to right) represent the electrostatic interaction energies calculated with Eq S12 of slabs with (1) a combination of real charges and their image charges from image surface 1 (top of slab), (2) a combination of real charges and their image charges from image surface 2 (bottom of slab), (3) the real charges, (4) the image charges from image surface 1, and (5) the image charges from image surface 2.

Table S1. Peaks and valleys in the intrinsic electron density profile, their centers and areas (integral of the peak or valley region).[1]

$ErCl_3$ concentration (M)	1st peak center (Å)	1st peak area (e Å^{-2})	valley center (Å)	valley area (e Å^{-2})	2nd peak center (Å)	2nd peak area (e Å^{-2})
0.2	10.5 [-8, +7]	0.018 [-5, +3]				
0.5	8.32 [-7, +10]	0.050 [-6, +7]	14.0 [-1, +1.4]	-0.003 [-2, +3]		
0.74	7.96 [-12, +12]	0.072 [-8, +30]	12.0 [-1.5, +0.6]	-0.012 [-8, +5]	16 [-3, +1.2]	0.002 [-2, +2]
1.0	7.44 [-8, +10]	0.110 [-12, +12]	12.1 [-3, +2]	-0.034 [-3, +3]	16.7 [-6, +5]	0.010 [-3, +3]

[1]The peaks and valleys that are not shown in the table have zero area within error bars (+/- 0.001 e Å^{-2}). Quoted standard deviations apply to the highest accuracy or underlined digits (e.g., 5.41 [-2, 2] refers to 5.41 ± 0.02).

Supporting Information References:

1. Patterson, A. H., A Fourier Series Method for the Determination of the Components of Interatomic Distances in Crystals. *Phys. Rev. A* **1934,** *46*, 372–376.
2. Tidswell, I. M.; Ocko, B. M.; Pershan, P. S.; Wasserman, S. R.; Whitesides, G. M.; Axe, J. D., X-Ray Specular Reflection Studies of Silicon Coated by Organic Monolayers (Alkylsiloxanes). *Phys. Rev. B* **1990,** *41*, 1111-1128.
3. Allen, M. P.; Tildesley, D. J., *Computer Simulation of Liquids*. Clarendon: Oxford, 1987.
4. Darden, T.; York, D.; Pedersen, L., Particle Mesh Ewald - an N.Log(N) Method for Ewald Sums in Large Systems. *J Chem Phys* **1993,** *98* (12), 10089-10092.
5. Essmann, U.; Perera, L.; Berkowitz, M. L.; Darden, T.; Lee, H.; Pedersen, L. G., A Smooth Particle Mesh Ewald Method. *J Chem Phys* **1995,** *103* (19), 8577-8593.
6. Aguado, A.; Madden, P. A., Ewald Summation of Electrostatic Multipole Interactions up to the Quadrupolar Level. *J Chem Phys* **2003,** *119* (14), 7471-7483.
7. Toukmaji, A.; Sagui, C.; Board, J.; Darden, T., Efficient Particle-Mesh Ewald Based Approach to Fixed and Induced Dipolar Interactions. *J Chem Phys* **2000,** *113* (24), 10913-10927.
8. Molina, J. J.; Duvail, M.; Dufreche, J.-F.; Guilbaud, P., Atomistic Description of Binary Lanthanoid Salt Solutions: A Coarse-Graining Approach. *J. Phys. Chem. B* **2011,** *115*, 4329-4340.
9. Yeh, I.-C.; Berkowitz, M. L., Ewald Summation for Systems with Slab Geometry. *J. Chem. Phys.* **1999,** *111*, 3155-3162.
10. Kawata, M.; Mikami, M., Rapid Calculation of Twp-Dimensional Ewald Summation. *Chem. Phys. Lett.* **2001,** *340*, 157-164.